A&A 372, L61–L64 (2001)
DOI: 10.1051/0004-6361:20010660

Astronomy & Astrophysics

Letter to the Editor

Asymmetries in the HD 141569 circumstellar disk⋆

D. Mouillet[1], A. M. Lagrange[1], J. C. Augereau[1,2], and F. Ménard[1,3]

[1] Laboratoire d'Astrophysique de l'Observatoire de Grenoble, Université J. Fourier/CNRS, BP 53, 38041 Grenoble Cedex 9, France
[2] DSM/DAPNIA/Service d'Astrophysique, CEA/Saclay, 91191 Gif-sur-Yvette, France
[3] Canada-France-Hawaii Telescope Corporation, PO Box 1597, Kamuela, HI 96743, USA

Received 15 January 2001 / Accepted 9 May 2001

Abstract. We present HST/STIS coronagraphic observations of the disk around HD 141569. The data, with a spatial resolution and signal to noise higher than those previously obtained with HST/NICMOS2 allow a more detailed insight in the system. They reveal a very structured system, in which two ring-like structures at distances ≃200 and 325 AU from the star are the most prominent features. The region between 125 and 175 AU is clearly devoid of material. An arc-like structure is also detected at about 250 AU, as well as a diffuse extended emission, both on the North side of the disk. The system appears to be highly asymmetrical, both with respect to its major and minor axes. Surprisingly, the brightness asymmetry with respect to both axes in the inner and outer parts of the disk is reversed. Possible explanations to the asymmetries include anisotropic scattering and/or non axisymmetrical distribution of the dust within the system. It is shown that anisotropic scattering cannot alone be responsible for all observed asymmetries. It is concluded that HD 141569 disk is non axi-symmetrical. Eventhough no detailed modeling is given in this observational paper, it is probable that the sculpting and brightness properties of the disk are due to the gravitational perturbation of a massive body.

Key words. stars: circumstellar matter – stars: HD 141569, β Pictoris, planetary formation, circumstellar disks, young stars

1. Introduction

The circumstellar protoplanetary disk around the young (5 ± 3 Myr, Weinberger et al. 2000) star HD 141569 has been identified as a possible transition case between those found around young objects and those around more evolved stars such as β Pictoris. Such disks are believed to contain the traces of planet formation. They are in a stage where planetesimals are numerous and planets may have already formed. In a broad evolutionary sense, they represent an evolved stage compared to the disks around young stars such as Classical T Tauri stars. They remain however much younger than the dust free planetary systems identified by radial velocity searches.

First HST/NICMOS2 1.6 μm coronagraphic observations revealed (Augereau et al. 1999) a dust ring peaked at 325 AU from the star (assuming a distance of 99 pc, van den Ancker et al. 1998) and inclined at 37.5°±4.5° to the line of sight. This wide ($FWHM \simeq 150$ AU) annular structure, confirmed by other HST/NICMOS2 1.1 μm data (Weinberger et al. 1999), scatters a small fraction of the stellar light (a few 10^{-3}) indicating that this dust population is optically thin. Weinberger et al. (2000) interpret the disk asymmetry with respect to the major axis as being due to weak anisotropic dust scattering properties.

The dust distribution inside the main resolved structure was uncertain. Bright patterns in the North–Northeast side of the 1.6 μm images, superimposed to secondary diffraction spikes, did not have any counterpart in the Southern side brighter than ∼18.5 mag arcsec^{-2} whereas the 1.1 μm images revealed a continuous second annulus at about 185 AU (Weinberger et al. 1999). Finally, (at least) a third dust population inside the first hundred of AU was inferred by SED fitting (Augereau et al. 1999) and later on detected in thermal emission at 18.2 μm (Fisher et al. 2000).

Clearly, higher spatial resolution images with higher signal-to-noise were needed to further progress in the knowledge of this system, in particular on its structure. This motivated new observations with STIS, at optical

Send offprint requests to: D. Mouillet,
e-mail: mouillet@obs.ujf-grenoble.fr

⋆ Based on observations with the NASA/ESA Hubble Space Telescope, obtained at the Space Telescope Science Institute, which is operated by the Association of Universities for Research in Astronomy, Inc. under NASA contract No. NAS5-26555.

Table 1. Journal of observations. UT time refers to UT start time. CR refers to number of detector read-outs (to allow Cosmic Rays rejection and to avoid saturation). The respective Hipparcos visual magnitude of HD141569 and the comparison star are 7.13 ± 0.4 and 5.69 ± 0.02.

Star	UT time	Wedge	Exp. time	CR
HD 141569	10:30:42	1.8″	1509 s	5
HD 141569	11:00:11	1.0″	410 s	8
HD 129433	12:12:44	1.8″	755 s	8
HD 129433	12:39:43	1.0″	124 s	8

wavelengths. We present (Sect. 2) data obtained with this instrument. The results are presented in Sect. 3 and briefly discussed in Sect. 4.

2. The data

2.1. Journal of observations

STIS coronagraphic images of HD 141569 have been taken on the 4th of August 2000 under programme ID 8674 (see Table 1). Central wavelength of the unfiltered aperture 50CCD is 5850 Å and $FWHM$ is 4410 Å. Taking into account the system response and target spectrum, the overall optical diffraction-limitted angular resolution obtained for this object is 44 mas only. Even if degraded by detector undersampling, these observations provide better angular resolution than previous ones in near IR. The detector has a 50 mas pixel size and provides a total FOV of $52'' \times 52''$ (STIS Instrument Handbook 1999). Two wedge sizes were chosen, one with a 1″ width (wedge B1.0) and the other with a 1.8″ width (wedge B1.8). A special care was taken to also position the two HD 141569 closest identified companions, located at about 7.5″ and 9″, behind the wedge in order to allow deep imaging.

To remove the PSF wings, we used a comparison star, HD 129433, of spectral type (B9.5V) similar to that of HD 141569, with the same masks configuration (see Table 1) in the following orbit. In order to obtain high dynamic range imaging, the detector conversion gain of 4 e^-/DN is selected even if a low-level video noise is expected with a typical amplitude of 1 DN at each read-out. The total exposure time is splitted into several detector read-outs in order to enable cosmic ray (CR) rejection.

2.2. Data reduction

After corrections for detector effects (bias, dark, flatfield, CR rejection), the data reduction aims at subtracting the residual coronographic PSF wings in order to distinguish much fainter circumstellar emission (Fig. 1). This subtraction uses the point-like comparison star observed at the same wedge position, after fine recentering and flux scaling. As observed by Grady et al. (1999, 2000) or Schneider et al. (2001) on respectively HST/STIS and NICMOS coronographic data, the comparison of diffraction spikes location and brightness enables the accurate determination of recentering and flux scaling parameters. The HD141569/HD129423 spikes flux ratio, measured over the range from 6 to 20 arcsec from the star, is 0.272 ± 0.002 (consistently for both wedges), corresponding to $\Delta m = 1.413 \pm 0.006$ (which is compatible but actually difficult to compare at this level of accuracy with the stars ΔV because of the present much wider spectral reponse of the system aperture).

Note that an error on the PSF subtraction has an impact on the photometry of circumstellar features. Such effects can be seen on the profiles presented in Fig. 3 where the scalings applied are set to match the 3 σ limit, i.e. 0.266 and 0.278. Admittedly, observing the source with various telescope roll angles would enable to reduce the image area blinded by the diffraction spikes and coronographic wedge (Grady et al. 1999); however this was made difficult and time consuming in the current case due to the additionnal necessity to also hide the companions behind the wedge.

3. Results

3.1. Wedge B1.0

Figure 2 shows the final image of the disk when using the scaling factor 0.272. More quantitatively, Fig. 3 shows the radial distribution of the disk brigthness, azimuthally averaged over 16° wide angular sectors at respective PA of 16° and 159°. These sectors are chosen because they are symmetrical with respect to the disk minor axis, and located apart from areas covered by diffraction spikes and coronographic wedges. These data reveal a highly structured system, with the following characteristics:

- two elliptical structures are clearly seen as the most prominent features at a position angle $357° \pm 2$. We can fit to these structures ellipses with a similar aspect ratio of 1.75 ± 0.05. Assuming circularity, this ratio corresponds to an inclination of $55° \pm 1.2$ from pole-on orientation. The first ring peaks at 200 ± 5 AU and the $FWHM$ is about 50 AU. The second structure peaks at 325 ± 5 AU from the star, but is much more diffuse, especially in the NE direction. Inside the first one, the flux strongly decreases and remains fainter than 19 mag/arcsec^2 down to the limit of the wedge, at 125 AU;
- a narrow ($FWHM \sim 25$ AU) arc-like structure is seen in the NE direction, with the same ellipticity as the rings, and located at 250 AU from the star;
- an extended diffuse emission is also present in the same side of the disk, up to more than 600 AU. The brightness decrease of the disk (measured over the 350–600 AU range) is much steeper to the South direction than it is to the North direction, with respective power-law indexes -6.2 ± 0.2 and -2.9 ± 0.1 (Fig. 3);
- strong brightness asymmetry is observed with respect to minor axis (factor ∼2 at 200 AU, and 1.5 at 325 AU). It is evidenced best in Fig. 3. Noticeably, the asymmetry is reversed from one "ring" to the other.

Brightness asymmetry with respect to major axis is much weaker (factor ≤ 1.2);
– the two best-fitting ellipses are not centered on the same point, but offset by $0.2''$ (20 AU).

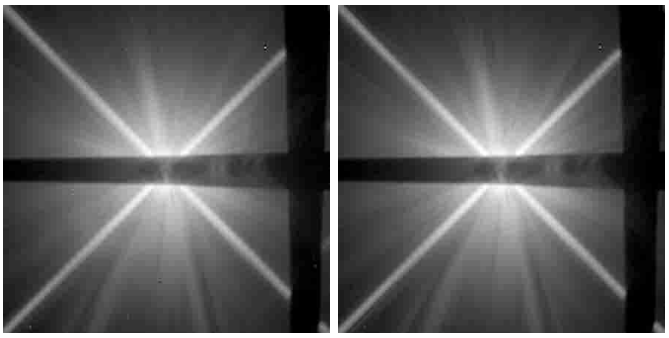

Fig. 1. Images of HD141569 (left) and the comparison star HD129433 (right) under the coronographic wedge (position B1.0) in logarithmic scale. The field of view is $11''$.

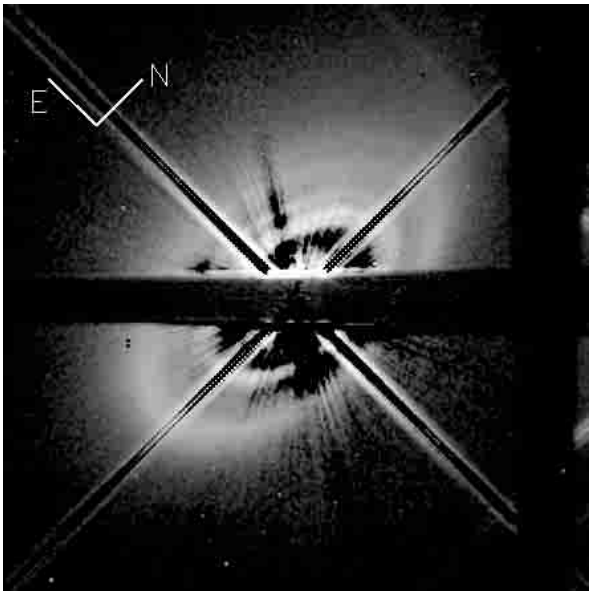

Fig. 2. PSF-subtracted image of the HD 141569 system (wedge B1.0) in logarithmic scale. The field of view is $11''$.

3.2. Wedge B1.8

The images obtained with wedge B1.8 consistently lead to the same results and conclusions (Fig. 4). In particular, the two elliptical and asymmetric structures are present, eventhough the innermost one is closer to the wedge. The arc-like structure is also confirmed, as well as the diffuse emission.

4. Discussion and concluding remarks

Our new images of HD141569 were obtained in the optical, at an effective wavelength of 585 nm. They provide

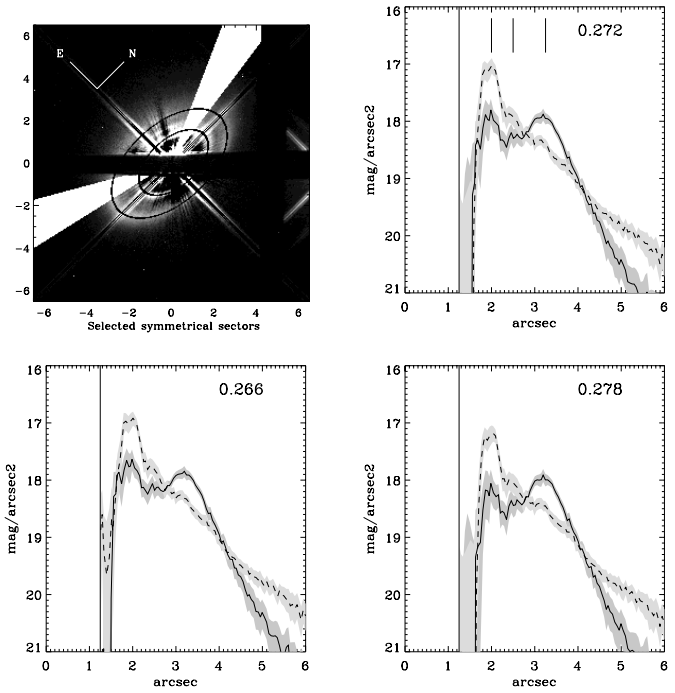

Fig. 3. Radial profiles of the disk in averaged over two angular sectors, which are symmetrical with respect to the disk minor axis. These sectors are represented on the upper left scheme (superimposed on the underlying disk image). Profiles extracted from the Wedge B1.0 data are represented for different flux scaling ratios: 0.272 (upper right), and the lower and higher estimations at 3 σ 0.266 and 0.278 (lower figures). The side to side asymmetries, reversed for the 2 rings are clearly seen (full line: southern sector ; dashed lined: northern sector). Grey areas indicate the statistical uncertainty of the profiles (pixel to pixel brightness standard deviation over each elliptical arc). Vertical lines indicate the distances corresponding to main structures (at 200 and 325 AU) and to the arc-like structure (250 AU).

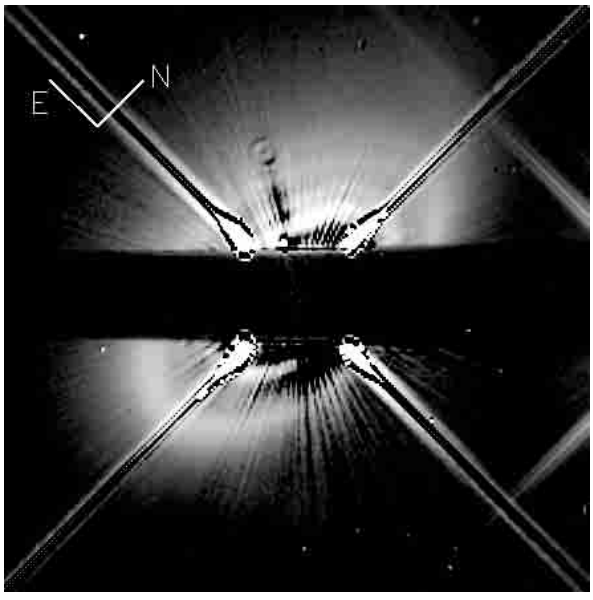

Fig. 4. Image obtained with the $1.8''$ wedge (same field of view).

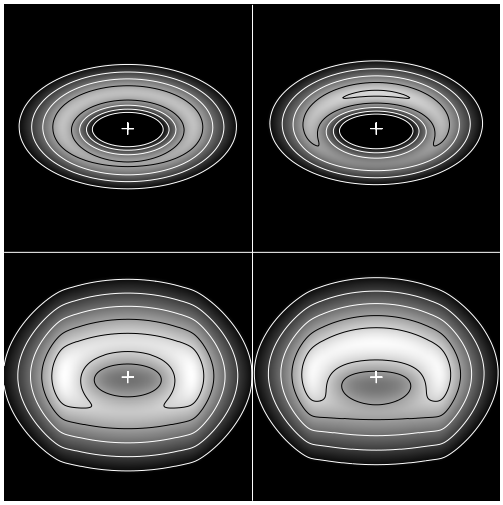

Fig. 5. Simulation of scattered light observations of an axisymmetrical optically thin disk. Contours separation is one magnitude. The disk inclination is 55° from pole-on. Images asymmetries with respect to major axis is due to scattering anisotropy: $|g| = 0.1$ (left) and 0.3 (right). No asymmetry with respect to minor axis can be obtained under these assumptions. The geometrical opening angle of dust distribution is either 5° (top) or 20° (bottom).

better angular resolution than the images of Weinberger et al. (1999) (at 1.1 μm) and Augereau et al. (1999) (at 1.6 μm). Our images fully confirm and improve the previous data showing an outside ring at about 325 AU (Weinberger et al. 1999, Augereau et al. 1999) and an inner one at about 200 AU (Weinberger et al. 1999). The improved resolution and contrast also evidence an inner region devoid of material (fainter than 19 mag/arcsec^2) from 175 down to 125 AU, where the wedge forbids further inspection. This shows that the hot population inferred by Augereau et al. (1999) and necessary to account for the SED shape at 10 μm is closer than 125 AU. This is also compatible with the thermal infrared images obtained by Fisher et al. (2000).

Brightness asymmetries can be a priori due to anisotropic scattering of the light by the grains and/or a non-axisymmetrical distribution of the grains within the disk. We first investigate whether an axisymmetrical dust distribution may be compatible with observations. An axisymmetrical system of grains with non isotropic scattering properties, inclined with respect to the line of sight, would produce brightness asymmetries with respect to the major axis. This effect is illustrated in Fig. 5, where scattering anisotropy is characterized by the value of the g parameter in the Henyey & Greenstein (1941) phase-function model.

We first conclude from the comparison with simulations that in order to be able to distinguish the observed sharp structures in the disk structure, the actual dust distribution needs to be quite geometrically thin (opening angle $\leq 5°$). Second, observed dust grains show only moderate scattering anisotropy ($|g| < 0.3$) in order to reproduce the asymmetry with respect to the major axis. No radial change of brightness asymmetry with respect to the minor axis is expected unless the grain properties change radially. Consequently, optical properties of the grains cannot alone produce asymmetries with respect to the minor axis. This leads us to conclude that non axisymmetrical dust distribution is needed on a large range of distances from the star to produce the brightness asymmetry of the inner ring at 200 AU, the "arc-like" structure at 250 AU, the extended emission in NE direction up to more than 600 AU. This could also probably account for the observed offsets between the centers when trying to fit the images with projection of rings.

Given the overall view of the system, one might think of two configurations giving non axisymmetrical distributions: the dust is distributed along ellipses with non zero eccentricities, or the rings are circular but the material is non uniformly azimuthally distributed. It is not possible to distinguish between both situations. In any case, the very non axisymmetrical distribution of the material within the system is a strong indication of on going gravitational perturbation by a companion. Modeling of such a situation is certainly out of the scope of the present paper and will be presented in a forthcoming one.

Acknowledgements. We wish to thank J. Papaloizou for very useful discussions, and the STSCI support (in particular P. Royle) for the support in the observation preparation.

References

Augereau, J. C., Lagrange, A. M., Mouillet, D., & Ménard, F. 1999b, A&AL, 350, 51

Fisher, R. S., Telesco, C. M., Piña, R. K., Knacke, R. F., & Wyatt, M. C. 2000, ApJL, 532, L141

Grady, C. A., Woodgate, B., Bruhweiler, F. C., et al. 1999, ApJL, 523, L151

Grady, C. A., Devine, D., Woodgate, B., et al. 2000, ApJ, 544, 895

Henyey, L. G., & Greenstein, J. L. 1941, ApJ, 93, 70

Schneider, G., Becklin, E. E., Smith, B. A., et al., AJ, 121, 525

Van den Ancker, M. E., de Winter, D., & Tjin A Djie, H. R. E. 1998, A&A, 330, 145

Weinberger, A. J., Becklin, E. E., Schneider, G., et al. 1999, ApJL, 525, 53

Weinberger, A. J., Rich, R. M., Becklin, E. E., Zuckerman, B., & Matthews, K. 2000, ApJ, 544, 937

STIS Instrument Handbook v3 (STSCI, Science Support Division) 1999